Early and Delayed STAT1-Dependent Responses Drive Local Trained Immunity of Macrophages in the Spleen

Aryeh Solomon[1], Noa Bossel Ben-Moshe[1], Dotan Hoffman[1], Sebastien Trzebanski[1], Dror Yehezkel[1], Leia Vainman[1], Mihai Netea[2,3], Roi Avraham[1]

1. Department of Immunology and Regenerative Biology, Weizmann Institute of Science, 7610001 Rehovot, Israel.
2. Department of Internal Medicine and Radboud Center for Infectious Diseases, Radboud University Medical Center, Nijmegen, Netherlands.
3. Department of Immunology and Metabolism, Life and Medical Sciences Institute, University of Bonn, Bonn, Germany.

Abstract

Trained immunity (TI) is the process wherein innate immune cells gain functional memory upon exposure to specific ligands or pathogens, leading to augmented inflammatory responses and pathogen clearance upon secondary exposure. While the differentiation of hematopoietic stem cells (HSCs) and reprogramming of bone marrow (BM) progenitors are well-established mechanisms underpinning durable TI protection, remodeling of the cellular architecture within the tissue during TI remains underexplored. Here, we study the effects of peritoneal Bacillus Calmette–Guérin (BCG) administration to find TI-mediated protection in the spleen against a subsequent heterologous infection by the Gram-negative pathogen *Salmonella* Typhimurium (*S*.Tm). Utilizing single cell RNA-sequencing and flow cytometry, we discerned STAT1-regulated genes in TI-associated resident and recruited splenic myeloid populations. The temporal dynamics of TI were further elucidated, revealing both early and delayed myeloid subsets with time-dependent, cell type-specific STAT1 signatures. Using lineage tracing, we find that tissue-resident red pulp macrophages (RPM), initially depleted by BCG exposure, are restored from both tissue-trained, self-renewing macrophages and from bone marrow-derived progenitors, fostering long lasting local defense. Early inhibition of STAT1 activation, using specific JAK-STAT inhibitors, reduces both RPM loss and recruitment of trained monocytes. Our study suggests a temporal window soon after BCG vaccination, in which STAT1-dependent activation of long-lived resident cells in the tissue mediates localized protection.

Introduction

Trained immunity (TI) is defined as the capacity of innate immune cells to recall and modulate their subsequent responsiveness following prior exposure to a diverse array of stimuli[1]. Unlike the adaptive immune system, these changes are antigen-agnostic and are more reflective of sustained alterations in cellular and systemic states. TI has been demonstrated to directly reprogram the metabolic, transcriptional, and epigenetic state of monocytes and macrophages, generating heightened inflammatory capabilities in-vitro[1,2]. As the transient lifespans of these cells are weeks only, this alone is insufficient to explain the sustained protection generated by TI that can last from months to years. To address this limitation, current research has been focused on long-lived multipotent progenitor immune cells.

BCG vaccine (Bacillus Calmette-Guérin), an attenuated strain of *Mycobacterium bovis*, is a potent inducer of TI, which facilitate nonspecific protection against heterologous pathogens in both mice, primates, and humans[3,4]. The effects of intravenous (i.v.) BCG vaccination, where bacilli persist within the bone marrow (BM), drive the expansion of LSK+ hematopoietic stem cells (HSCs) and multipotent progenitors (MPPs)[4]. In conjunction, MPPs undergo biased differentiation towards myelopoiesis, increasing the proliferation of myeloid cells. These effects are driven primarily by interferon activation, particularly that of interferon-gamma (IFNγ) and its downstream transcription factors, STAT1 and IRF1, in MPPs and short-term HSCs, resulting in a transcriptional program of cell cycling (Cdk1, Cdk4, Ccnf) and histone modifications. Furthermore, these newly differentiated circulating cells have enhanced microbicidal properties[5,6]. Upon infection, in order to elicit protection against invading agents, trained progenitor immune cells from the BM interact within local immune cell compartments in the tissue. The nature of these interactions and how TI translates within the tissue and the local cellular architectures is not completely understood.

Most tissues harbor long-lived resident macrophages capable of self-renewal, independent of BM-derived precursors. These resident populations, including pulmonary alveolar macrophages, Kupffer cells in the liver and red pulp macrophages in the spleen, originate from embryonic erythro-myeloid progenitors[5]. Antimicrobial activity of resident populations control early stages of invasion by pathogens but are than depleted, and the niche is repopulated either by self-renewal[6] or by progenitors derived from the BM to maintain local functions[7]. Intriguingly, resident alveolar macrophages (AM) have been shown to undergo in-situ training, maintaining an altered phenotype over an extended period[10–12]. One

59 mechanism driving this training in-situ in AMs involves CX3CR1^{+} T cells, which have been implicated in
60 local reprogramming via IFNγ release. This process has been demonstrated to occur around three weeks
61 after initial BCG vaccination, after which interferon-driven responses occur across the organism,
62 including lung and BM, resulting in viral and mycobacterial protection. It remains unclear however, how
63 during TI, a bridge is formed between peripheral, resident cells and BM-derived recruitment of trained
64 myeloid cells.

65 In this study, we set out to investigate the interplay of circulating and tissue-level immune cells that
66 mediate protection and remodeling during TI. To induce tissue specific TI, we used a model of
67 intraperitoneal (i.p.) injection of BCG, which rapidly delivers the bacteria to target lymphatic organs
68 (*e.g.,* spleen), and measured protection against subsequent *Salmonella* Typhimurium (*S*.Tm) challenge.
69 Within the spleen's unique structure and cellular composition, we characterized STAT1-mediated, cell
70 type-specific TI signatures. We demonstrate that an initial depletion of resident red-pulp macrophages is
71 followed by replenishment by recruited trained monocytes and a local self-renewing population,
72 contributing to the maintenance of STAT1 signatures and long-lasting protection within the tissue.

73

74 Results

75 **Intraperitoneal BCG results in heterologous *S*.Tm protection and a distinct myeloid subsets with**
76 **signatures driven by STAT1.**

77 To establish an in-vivo BCG training model targeted to the splenic tissue, and assess the extent of cross
78 pathogen tissue protection conferred, we administered BCG-Pasteur[8] (5×10^{6} colony forming units (CFU))
79 or PBS as a control via i.p injection to 8-week-old female C57BL/6J mice. Following a two-week training
80 period, mice were challenged with *S*.Tm ($5x10^{5}$ CFU) through i.p inoculation (**Fig. 1A**). Mice were
81 sacrificed after twenty-four hours, and spleen homogenates were cultured on LB agar medium to
82 quantify *S*.Tm load using CFU (**Fig. 1B**). Relative to the control group, mice that received BCG exhibited
83 enhanced protection against *S*.Tm, with a four- to five-fold decrease in CFU, indicating TI-mediated
84 splenic protection.

85 For identification of transcriptional changes in splenic myeloid populations related to TI, we isolated
86 splenocytes and performed staining with CD11b, Ly6C, and F4/80 gating for myeloid mononuclear
87 phagocytes (MPs), including classical monocytes (CM) (CD11b^{+}Ly6C^{+}), and CD11b^{+} Ly6C^{-} MPs comprising

88 non-classical monocytes (NCM) and conventional dendritic cells (cDC), and also resident red pulp
89 macrophages (RPM) (CD11b$^-$ F4/80$^+$) (**Fig. 1C**, **Figure 1 — figure supplement 1A**). We observed an
90 overall expansion of the myeloid compartment due to training, with an increase in the CD11b$^+$ subset,
91 and a pronounced reduction of resident RPM (**Fig. 1D**). This observed loss of RPM is common during
92 infection and inflammation and has been previously described as the resident macrophage
93 disappearance reaction[9].

94 We next determined transcriptional alterations caused by TI across the myeloid compartment. CD11b$^+$
95 cells from trained and naïve mice were isolated by sorting and processed for single-cell RNA-sequencing
96 (scRNA-seq)[10]. K-nearest neighbor (K-NN) clustering differentiated six distinct cell types, designated as
97 CM, NCM, immature DC2 (cDC2), mature DC2 (mcDC2), neutrophils, and NK cells (**Fig. 1E**). The identity
98 of each cell type cluster was based on established transcriptional markers (**Fig. 1F**). Additional analysis
99 was performed to identify differentially expressed genes (DEG) unique to training (**Fig. 1G-I; Table S1**).
100 While most populations derived from control or trained mice clustered together by cell type, we
101 identified a subset of trained CM (CM-T) particular to BCG (**Fig. 1G**). These cells uniquely express a set of
102 inflammatory genes regulated by STAT1 activity, as part of the IFNγ response (*e.g.*, *Gbp2, Ly6a, Cxcl9*,
103 and *Irg1)* (**Fig. 1J**). Notably, these STAT1 activation genes are known to drive maturation and activation
104 of monocytes and macrophages, enhancing their antimicrobial response[11]. GBP2 (guanylate binding
105 protein 2), part of the broader GTPase family, is highly activated during IFNγ stimulation and can bias
106 macrophages to an inflammatory M1 state[12], as well as inhibit gram-negative intracellular bacterial
107 growth via disruption of the pathogen containing vacuole and pyroptosis induction[13]. CXCL9 (chemokine
108 ligand 9) is known to be involved in T cell and monocyte recruitment to infection sites and their
109 subsequent activation[14], and its role in trained immunity has been previously suggested, as it is a key
110 player in the formation of a pro-inflammatory milieu that facilitates rapid and efficient pathogen
111 clearance[15]. IRG1, an enzyme that catalyzes the production of itaconate, is a metabolite that triggers
112 metabolic reprogramming of MPs with both antimicrobial and immunomodulatory properties[16]. The
113 enhanced production of itaconate may further contribute to the protective effects of TI by directly
114 inhibiting pathogen growth and fine-tuning the immune response to prevent excessive inflammation[17].
115 However, the role of IRG1 in training is context dependent, as monocyte exposure to β-glucan exposure,
116 a common training ligand, has been demonstrated to block its activity and the subsequent accumulation
117 of itaconate[18].

118 *Stat1* and its downstream targets (*e.g.*, *Gbp2*, *Irf1,* and *Ly6a*), exhibited a pronounced elevation also in
119 other myeloid cells (**Figure 1 — figure supplement 1B**), aligning with an earlier report that BCG induces
120 BM and HSC remodeling via interferon signaling, resulting in STAT1 upregulation in progenitors[19].
121 However, not all populations were similarly activated in conjunction with STAT1-regulated genes, with
122 gene set enrichment analysis (GSEA) demonstrating differential pathway upregulation across cell types
123 (**Fig. 1I**). CM and mcDC2 primarily activated the IFNγ response, while complement associated genes
124 were enriched in mcDC2. NK cells alone showed minimal activation due to training across all detected
125 pathways (**Figure 1 — figure supplement 1B**).

126 We also observed increased SCA-1 (*Ly6a/e*) expression across the monocyte subsets and mcDC2, most
127 notably in NCM (**Fig. 1I**; **Figure 1— figure supplement 1B**). SCA-1 (stem cell antigen-1) is a
128 glycosylphosphatidylinositol-anchored cell surface protein commonly used as a marker for murine
129 hematopoietic stem and progenitor cells within the BM. The STAT1 signaling pathway has been shown
130 to be involved in the regulation of SCA-1 expression[20], suggesting a role for STAT1 in the modulation of
131 SCA-1 during development of TI. Recent studies have also demonstrated a link between SCA-1 and
132 inflammation, with its expression found to be upregulated on a specific subset of $Ly6C^+$ monocytes
133 during infection[21]. These $SCA\text{-}1^+$ monocytes exhibited a pro-inflammatory phenotype, characterized by
134 the production of inflammatory cytokines and chemokines, and were implicated in the amplification of
135 these responses. For $Ly6C^-$ NCM, the role of SCA-1 has not yet been studied.

136 In addition to the upregulation of inflammatory and antimicrobial genes, we also observed a significant
137 downregulation of specific genes in CM-T as a result of training, including *Ccr2*, *S100A8/9,* and *Ngp*.
138 CCR2, a chemokine receptor crucial for monocyte recruitment, was found to be downregulated in
139 response to IFNγ. This reduction in CCR2 expression is mediated by IFNγ-induced mRNA instability,
140 potentially serving to retain monocytes at the site of recruitment and dampen a positive feedback
141 loop[22]. Similarly, BCG has been shown in other contexts to reduce the expression of S100A8 and S100A9,
142 two calcium-binding proteins that can heterodimerize and stimulate IFNγ production in CD4+ T-cells via
143 an IL-10 dependent mechanism[23]. By suppressing their activity, runaway signaling and exhaustion is
144 avoided. Lastly, NGP (neutrophilic granule protein), has been implicated in the regulation of
145 inflammation through its ability to block NF-κB signaling[24]. The downregulation of these genes suggests
146 that trained immunity not only enhances pro-inflammatory responses but also modulates the
147 expression of key regulators to maintain a balanced immune response and prevent excessive
148 inflammation.

149

150 **Dynamics of TI-associated subsets and signatures indicates early and delayed kinetics**.

151 To gain insight into dynamic processes underlying splenic cell type-specific TI, we conducted a two-
152 month experiment, sacrificing mice at days 3, 14, 30, 45, and 60 post-vaccination with BCG (**Fig. 2A**). We
153 assessed BCG growth in BM and spleen, resistance to *S*.Tm infection, flow cytometry analysis with cell
154 type-specific training markers (CXCL9 and SCA-1), and bulk RNA-seq. Notably, protection against *S*.Tm
155 persisted for two months post-vaccination, albeit with waning resistance over time (**Fig. 2B**). While
156 intravenous (i.v) BCG delivery and localization in BM were crucial for robust training[19,25], our results
157 indicate that during i.p administration, direct BCG-immune cell interactions in the BM may not be
158 required, as no BCG bacteria within the BM could be detected (**Fig. 2C**). Conversely, in the spleen, we
159 isolated BCG at all time points, with CFU declining sharply by day 14, reaching the limit of detection by
160 day 30 with minimal bacterium remaining (**Fig. 2C**).

161 Flow cytometry analysis revealed a dynamic process during trained immunity (**Figure 2— figure**
162 **supplement 1A**). BCG exposure triggers a dramatic decline in RPMs at day 14, that subsides thereafter
163 (**Fig. 2D**, **Figure 2— figure supplement 1B**). At the same time, we observed rapid recruitment of CMs in
164 the spleen, starting already at day three after BCG, peaking at day 14 before returning to baseline (**Fig.**
165 **2D**). Early recruited CM expressed CXCL9, a marker gene of STAT1- mediated TI, which we observed was
166 most elevated at day 14 (**Figure 2— figure supplement 1C**). In a separate experiment to assess early
167 kinetics of CXCL9^{+} CM, we measured a significant increase of this subset already at five days post BCG
168 (**Figure 2— figure supplement 1D**), indicating an early recruitment of these cells due to the initial
169 response to BCG. NCMs exhibit a different TI signature and kinetic pattern. While their ratio initially
170 declines, they return to steady-state levels by day 30 (**Fig. 2D**). NCMs express SCA-1 (*Ly6a*), another
171 STAT1-regulated gene, which persists and remains highly elevated at all subsequent time points (**Figure**
172 **2— figure supplement 1C**). When challenged with a subsequent *S*.Tm infection at day 14, CXCL9
173 expression in CMs was increased, but these differences were entirely lost by day 60 (**Figure 2— figure**
174 **supplement 1E**). In contrast, SCA-1 expression in NCMs remained upregulated (**Figure 2— figure**
175 **supplement 1E**).

176 Notably, the expression of STAT1-mediated TI markers is not solely restricted to BM-derived myeloid
177 cells but also occurs in tissue-resident RPM. RPM loss is evident after 14 days of training (**Fig. 2D**),
178 together with increased expression of the STAT1-regulated CXCL9 (**Figure 2— figure supplement 1C, D**).

179 SCA-1^{+} RPM levels fluctuate, elevating at day 14 and increasing again at day 60. Given their pivotal role
180 in curbing the early replication of intracellular pathogens[26], such as *S*.Tm, and their long life span, as
181 opposed to CM and NCM[27], trained RPM could be an additional determinant in generating long-lasting,
182 localized tissue protection.

183 From the splenocytes collected during the kinetics experiment, we generated and analyzed bulk RNA-
184 seq data. Principal component analysis (PCA) displayed a substantial shift along PC1 due to BCG training
185 (**Figure 2— figure supplement 1F**). Examination of all differentially expressed genes (DEGs) between
186 BCG and PBS across these time points revealed the greatest transcriptional changes at day 14 and 30
187 (**Fig. 2E; Table S2**). To investigate the biological processes represented at these time points, GSEA was
188 performed. At day 14, we detected enrichment for IFNγ response, IFNα response, and IL6-JAK-STAT
189 signaling, with many genes shared across these pathways. In contrast, day 30 was characterized by
190 enrichment of E2F targets, G2M checkpoint, and heme metabolism (**Fig. 2E, F**). Within these terms,
191 especially for the IFNγ response, we noted that associated genes have differential expression patterns.
192 For example, *Irg1* upregulation is limited to day 14 (**Figure 2— figure supplement 1G**) returning to
193 control values for all subsequent time points. This is may reflect that IRG1 induction requires bacterial
194 phagocytosis and activation of the TLR-2/MYD88/NFKB axis[28]. Conversely, an increase in *Cxcl9*
195 expression is already observed by day 3, plateauing at day 14, and decreasing by day 30, mirroring it's
196 induction in CM-T in the flow cytometry analysis. Curiously, despite its loss in CM, the bulk
197 transcriptional expression of *Cxcl9* is still sustained after 2 weeks, though at reduced levels. This may be
198 attributed to its activity in other immune cells or regulatory mechanisms preventing further translation.
199 *Stat1* and its downstream target *Ly6a* (SCA-1) maintain high expression 2 months post vaccination
200 (**Figure 2— figure supplement 1G**). Several other interferon-regulated genes were also upregulated at
201 day 14, including the *Gbp* gene family, *Ifitm3*, and *Socs3* (**Fig. 2G**). GBPs are guanylate-binding proteins
202 involved in antimicrobial activity and inflammasome activation[29], while IFITM3 is an interferon-induced
203 transmembrane protein that plays a role in the antiviral response[30]. SOCS3, a suppressor of cytokine
204 signaling, particularly via IL-6/STAT3, is necessary component for mycobacterial infection control. By
205 blocking IL-6 signaling, SOCS3 allows for TNF and IL-12 signaling to occur, initiating CD4-dependent IFNγ
206 release[31]. Importantly, while the IFNγ response was reduced after 2 weeks, we detected sustained
207 upregulation of these genes for all subsequent time points (**Fig. 2H**), strengthening its role and that of
208 the JAK-STAT pathway in mediating the effects of TI.

209 Our findings also revealed that day 30 was enriched for cell cycling and heme metabolism (Fig. 2F).
210 Interestingly, RPM play a crucial role in iron homeostasis, recycling and storing iron from senescent
211 erythrocytes, preventing accumulation of free iron that can lead to ROS production, oxidative damage,
212 and pathogen utilization[32]. Given the dynamics of RPM loss by day 14, it is tempting to speculate that
213 their subsequent replenishment is reflected by these processes.

214 We then wanted to determine whether TI signatures in the spleen are due to recruitment of progenitors
215 from the BM or sustained local signals in the tissue. BCG or PBS were injected i.p into mice with either a
216 CD45.1 or CD45.2 background, respectively (**Figure 2— figure supplement 1H**). After two weeks, BM
217 was harvested from both, HSCs mixed 1:1, and injected into irradiated mice for BM transplant. Six weeks
218 post transfer, mice were sacrificed and myeloid cells in the spleen were assessed (**Figure 2— figure**
219 **supplement 1I**). Within each mouse, we found in the spleen a greater fraction of NCM expressed SCA-1
220 from trained donors relative to the naïve control (**Figure 2— figure supplement 1J**). CXCL9, which we
221 had previously observed in CM, was undetectable in the populations, possibly because its expression is
222 early and transient, as seen in the kinetics data.

223

224 **RPM niche is replenished by recruited trained monocytes and by local training of tissue-resident**
225 **populations**.

226 We observed a substantial reduction in RPM numbers upon BCG, followed by the expression of STAT1-
227 mediated TI markers in RPMs. We hypothesized that upon BCG, two possible scenarios for training and
228 replenishment of open niche are possible. The first is self-renewal by the remaining local tissue-resident
229 macrophages who are trained within the tissue, while the other is that BM-derived trained monocytes
230 differentiate and repopulate the open niche. While BM-derived macrophages may adopt signatures and
231 function of their local counterparts, they may also retain aspects of their origin, particularly enhanced
232 inflammatory capacities (**Fig. 3A**). To investigate this, we employed MS4A3^{Tdtm};CX3CR1^{GFP} reporter
233 mice[33] with a knock-in flox-cre system to selectively label BM-derived monocytes with TdTomato
234 fluorescence. As MS4A3 is distinctly expressed in granulocyte-monocyte progenitors (GMP), only this
235 lineage will be TdTomato positive. These mice were administered BCG or PBS-i.p following the training
236 protocol and sacrificed two weeks later (**Fig. 3B**). Effective labeling was determined by flow cytometry,
237 measuring the fraction of MP expressing TdTomato and/or CX3CR1 (**Figure 3— figure supplement 1A**).
238 As expected, the monocyte population were primarily double positive (**Figure 3— figure supplement**

239 **1B**). Intriguingly, training increased the percentage of labeled cells across monocytes, suggesting a
240 potential lineage bias towards granulocyte-monocyte progenitors (GMPs). This observation is consistent
241 with prior studies demonstrating that various microbial components can induce short-term
242 differentiation biases in monocytes derived from GMPs or MDPs (monocyte-dendritic progenitors),
243 endowing them with neutrophil- or dendritic cell-like properties[34].

244 For the majority of RPM, we expected minimal TdTomato expression, representative of self-
245 replenishment during homeostasis. However, already within the control we observed that ~16% of the
246 population were labeled (**Fig. 3C**). When this population was depleted during training, an even greater
247 fraction was positively labeled. Accordingly, even under steady-state conditions, BM-derived cells
248 contribute to the resident niche, but when sufficiently diminished post vaccination, active
249 replenishment from the BM does occur.

250 To determine whether Tdtm$^+$ BM-derived RPM acquired a distinct transcriptional profile due to training
251 compared to the native Tdtm$^-$ population, we sorted Tdtm$^+$ RPMs, Tdtm$^-$ RPMs, and Tdtm$^+$ CM and NCM,
252 from both trained and naïve conditions. These sorted cell populations were then subjected to bulk RNA-
253 seq and subsequent analysis. Crucially, training associated genes were differentially expressed across all
254 sorted cell types (**Fig. 3D**; **Figure 3— figure supplement 1C; Table S3**). When evaluating specific DEGs
255 upregulated across trained RPM, we identified five gene clusters that varied between CM, NCM, and
256 RPM, as well as genes primarily upregulated in Tdtm$^+$ or Tdtm$^-$ RPM (**Fig. 3E**). Cluster I is composed of
257 MHCII-associated genes (*H2-Aa*, *H2-Eb1*, CD72, etc.), and is enriched in NCM and RPM cells, indicating
258 enhanced antigen presentation that may facilitate the activation of humoral immunity. Cluster II consists
259 of the STAT-1 regulated TI hallmark genes, including *Cxcl9*, *Gbp2* and *Stat1* and is upregulated in all
260 trained subsets. Genes in Cluster III, such as *Aif1*, *Fpr1*, and *Hk3*, are primarily observed in trained RPM
261 and are involved in response to tissue damage/disruption and immune infiltration. AIF1 is an established
262 marker of macrophage activation and is functionally involved in phagocytosis and membrane ruffling[35].
263 Similarly, FPR1, a formyl peptide receptor, induces chemotaxis, phagocytic uptake, and reactive oxygen
264 species (ROS) production[36]. Cluster IV is upregulated in BCG Tdtm$^-$ RPM, though the role of most genes
265 detected in this cluster remains unknown in regard to their tissue-specific function and activation.
266 Interestingly, *CD8A* expression, typically relegated to lymphocytes, was observed in this cluster. In
267 monocytes, CD8A can co-engage with FcR, resulting in TNF release[37]. Lastly, cluster V, which is primarily
268 activated in CM regardless of training, was also upregulated in RPM due to BCG. Three of the genes
269 within the cluster, *Anxa1*, *Vim*, and *Wfdc17*, have all been shown to dampen excess inflammatory

270 responses through various mechanisms, including suppressing oxidative stress and promoting local
271 resolution[38–40].

272 GSEA performed across all upregulated genes revealed that the IFNγ response was enriched, followed by
273 IFNα response, allograft rejection, and JAK-STAT signaling (**Fig. 3F**). Although the IFNγ signature was
274 most prominent in CM, it was also observed in NCM and in the Tdtm^{+} RPM. This finding suggests that
275 engrafted monocytes differentiating within the niche may maintain a more inflammatory phenotype
276 and a heightened sensitivity to IFNγ activation. However, the BM-derived RPM are not the sole
277 population responsive to training, as the local fraction also upregulates the same genes in clusters I-III.
278 Notably, RPM, as a whole, demonstrate a greater capacity to upregulate the expression of many
279 interferon genes, including *Cxcl9* and *Stat1* (**Figure 3— figure supplement 1D**). Taken together, our
280 results indicate that BCG can reprogram populations and generate training via two separate routes.
281 First, the recruitment of trained progenitors and monocytes within the spleen, which differentiate
282 within a vacant niche, retaining their trained identity. Second, activation directly within the spleen in the
283 context of native tissue-resident RPM, generating tissue-specific protection.

284

285 **Transient IFNγ-STAT1 inhibition prevents TI signatures and splenic infection resistance.**

286 We observed that STAT1 signaling holds a critical role in training, with its regulated gene expression
287 elevated across the myeloid population. However, BCG is an intact attenuated bacterium that can
288 activate numerous PRRs. To evaluate whether STAT1 is necessary for TI signatures and protection, we
289 vaccinated STAT1-KO mice[41] with either PBS or BCG-i.p (**Figure 4— figure supplement 1A**). After a two-
290 week period, we assessed the myeloid population and STAT1 regulated genes. We observed a complete
291 absence of expression for both CXCL9 and SCA-1 across myeloid populations (**Figure 4— figure**
292 **supplement 1B**). This aligns with previous findings that demonstrated compromised acquisition of
293 trained immunity in IFNγR$^{-/-}$ mice[19]. Interestingly, RPM, typically depleted following BCG inoculation,
294 remain preserved in STAT1-KO mice (**Figure 4— figure supplement 1C**), suggesting that STAT1-mediated
295 pathways are involved in triggering the cellular death processes that occur during BCG interaction
296 and/or engulfment.

297 There is however a significant limitation in this mouse model, as STAT1$^{-/-}$ leave mice highly susceptible to
298 infection due to a severe compromise of immune homeostasis, limiting our ability to assess TI-mediated
299 protection upon *S*.Tm challenge. In light of our findings that STAT1 signaling is activated shortly after

300 BCG administration, we sought to transiently restrict STAT1 activity at these early time points, also
301 enabling us to investigate the effect of inhibition of STAT1 signaling on training and protection, without
302 affecting STAT1 activation during a secondary *S*.Tm challenge. To accomplish this, we used Fedratinib, a
303 specific inhibitor of JAK2 activation of STAT1 through IFNγ signaling[34], and Deucravacitinib, a specific
304 inhibitor of TYK2 activation of STAT1/STAT2 through IFNα/β signaling[42]. First, we administered DMSO
305 (control), Deucravacitinib, and Fedratinib i.p followed by BCG or PBS-i.p four hours after. These
306 inhibitors were then injected daily via i.p for the following four days, followed by a subsequent nine-day
307 rest period (**Figure 4— figure supplement 1D**). At the two-week mark, splenocytes were extracted from
308 all mice and analyzed by bulk RNA-seq. Only Fedratinib, not Deucravacitinib, resulted in inhibition of
309 STAT1-mediated TI signatures (**Figure 4— figure supplement 1E; Table S4**).

310 We then repeated this experiment, focusing on training phenotypes in the spleen and BM. At the two-
311 week mark, splenocytes were extracted from all mice for flow cytometry analysis, with CXCL9 utilized as
312 a marker for STAT1-mediated TI signature in monocytes. As observed in the transcriptional response,
313 only Fedratinib ablated expression of CXCL9 in CM (**Figure 4— figure supplement 1F**). We also sought to
314 determine if these effects were localized solely to the tissue, or if they extended to progenitors in the
315 BM, which expand upon BCG exposure[19]. To ascertain this, we isolated BM from the femur, measuring
316 the percent of LSK^+ HSCs (**Figure 4— figure supplement 1G**). Here too, only Fedratinib resulted in
317 suppressing their expansion to levels comparable to the control (**Figure 4— figure supplement 1H**).
318 Conversely, perturbation of IFNα/β signaling with Deucravacitinib lead to no observable changes on
319 trained subsets, suggesting that it is not involved in our BCG-i.p model. Type-I interferon has been
320 established as a training signaling pathway in other contexts, as observed with β-glucan[43], *Candida*
321 *Albicans*[44] and LPS[45].

322 In order to prove that early STAT1 inhibition is sufficient to block the TI protective phenotype, and not
323 just downstream markers, we repeated the inhibitor regime with control or trained mice receiving
324 either Fedratinib or DMSO, with or without *S.*Tm infection after 2 weeks (**Fig. 4A**). We then extracted
325 spleens to measure splenic expansion, splenoctye population levels and marker expression with flow
326 cytometry, bulk splenocyte transcription, and *S*.Tm susceptibility. Importantly, while we observed no
327 differences in CFU between control mice with or without Fedratinib, trained mice receiving Fedratinib
328 were significantly more susceptible to infection (**Fig. 4B**). Treatment with Fedratinib resulted in
329 diminished recruitment and splenocyte expansion, causing an appreciable reduction in spleen size
330 comparable to the control (**Figure 4— figure supplement 1I**). Accordingly, the balance of monocytes

331 ratios, particularly NCM, was shifted to levels similar to those observed in the DMSO control (**Fig. 4C**). In
332 conjunction, the expression of CXCL9, an early training marker, was reduced in both CM and RPM (**Fig.**
333 **4D**). Finally, RPM, which typically undergo depletion after training, exhibited significantly enhanced
334 survival, similar to the observations in STAT1-KO mice.

335 To probe the effects of Fedratinib inhibition beyond myeloid expansion and marker acquisition, we
336 conducted bulk RNA sequencing on total splenocytes isolated from all experimental conditions. PCA of
337 the resulting data revealed two major axes of divergence among the populations: PC1, associated with
338 training, and PC2, associated with the response to *S*.Tm (**Figure 4— figure supplement 1J**). While the
339 PBS-i.p mice treated with either DMSO or Fedratinib were grouped together, the BCG-i.p samples
340 treated with Fedratinib clustered distinctly, shifting closer to the PBS control group. Analysis of
341 downregulated DEGs identified the IFNγ response as the most significantly affected pathway due to
342 JAK2 inhibition by Fedratinib. This included its downstream effector *Stat1*, and other key STAT1-
343 regulated trained immunity genes, such as *Cxcl9/10*, *Irf1*, *Gbp2*, and *Irg1*, across all treated mice (**Fig. 4E,**
344 **F; Table S5**). To further validate our findings and ensure that the loss of the trained immunity signature
345 was not solely a result of blocking other JAK2-associated pathways, we repeated the inhibitor
346 experiment using recombinant α-IFNγ. Mice were given either α-IFNγ or an isotype control after BCG or
347 PBS vaccination, with injections on days 0, 2, and 4, and assayed two weeks post-vaccination. Upon
348 sorting and sequencing CM and RPM from these treated mice, we found that the STAT1 regulated TI
349 signatures were completely ablated with early inhibition (**Figure 4— figure supplement 1K-L**).
350 Importantly, when we plated spleen homogenates at the two-week interval, we still detected viable
351 BCG, demonstrating that training can be blocked even when BCG remain in the tissue (**Figure 4— figure**
352 **supplement 1M**).

353 Thus, the impact of Fedratinib and α-IFNγ treatment on the TI phenotype further underscores the
354 pivotal role of IFNγ and the JAK2-STAT1 axis in orchestrating the early programs and signatures required
355 for long-term local and recruited myeloid populations within the tissue. When compromised,
356 remodeling is suppressed and so too protection. Crucially, even though its administration was early and
357 removed after only five days administration, inhibition occurred. This indicates that the acquisition of TI
358 in the tissue occurs within a critically narrow temporal window.

359

360 ## Discussion

361 TI, or innate immune memory, embodies the capacity of innate immune cells to remember past
362 encounters and modify their subsequent responses, triggered by diverse conditions and stimuli. In-vivo
363 these processes are sustained in progenitor cells within the BM to provide long term TI, with
364 differentiated cells inheriting this memory[19,46]. In this study, we set out to demonstrate how long-term
365 protection events in the BM affords training within the tissue through local interactions with resident
366 populations. We demonstrated how the immune effects of BCG vaccination are differentially imparted
367 across recruited trained monocytes from the BM and diverse MP populations within the spleen, the
368 temporal dynamics governing these processes, and the mechanisms necessary for them to be sustained
369 long-term.

370 We verified that BCG-i.p inoculation stimulates an expansion of myeloid MP, notably CM, within the
371 spleen. Our dissection of single-cell training signatures uncovered a fundamental program highlighting a
372 signature of IFNγ response and STAT1 regulated genes across diverse populations. By monitoring the
373 kinetics of training over an extended duration, we observed that the initial surge in CM recruitment is
374 confined to the first two weeks of training, potentially signaling inflammatory recruitment triggered by
375 BCG exposure and RPM loss. Concurrently, the presence $CXCL9^{+}$ CM-Ts starts to diminish at a similar
376 rate and is eventually lost, suggesting that these cells may be differentiated to trained MPs in the tissue.

377 The depletion of RPMs at 14 days post-vaccination sets in motion a series of complex cellular responses.
378 Notably, we observed an enrichment of heme metabolism at day 30, which may indicate an ongoing
379 process of RPM replenishment. This process typically involves two key mechanisms: the local expansion
380 and repopulation by native populations, and the recruitment of erythroid and myeloid progenitors,
381 including classical and non-classical monocytes, to the organ[47]. These recruited cells, particularly
382 monocytes, can differentiate within the niche, transitioning through a pre-RPM state via heme-mediated
383 pathways[48]. Interestingly, heme metabolism has also been implicated in the control and pathogenicity of
384 mycobacterial species, particularly *Mycobacterium tuberculosis* (MtB). During systemic infection, MtB
385 activates type I interferon (IFN-I) signaling, which, along with its own virulence factors, disrupts iron
386 transport and uptake[25].

387 The presence of TI markers not only in BM-derived myeloid cells such as CM and NCM, but also in RPM,
388 prompted us to uncover how these cells acquired this phenotype. Utilizing $Ms4a3^{TdTm}$ labeled mice, we
389 investigated whether trained RPM were being derived from cells originating in the BM. Unlike CM and
390 NCM, which are predominantly $TdTm^{+}$, RPM express this lineage tracing marker at steady state around
391 16%, which was further increased with training. Probing the transcriptional profile of these cells also

392 revealed differences due to origin, with Tdtm$^+$ RPM demonstrating a heightened response to IFNγ
393 stimulation and elevated expression of STAT1. However, both populations exhibit significant
394 upregulation of TI-associated genes post-vaccination. These findings indicate that TI in RPM is not solely
395 due to BM-derived precursors filling a depleted niche but suggests a capacity for both resident and BM-
396 derived RPM to undergo training within the tissue itself. Considering the importance of these cells in
397 restricting early infection events[26], their capacity for training reveals an additional factor contributing to
398 the TI phenotype. While our examination was limited to a singular tissue-resident macrophage subset,
399 other splenic macrophages like marginal zone macrophages (MZMs) and marginal metallophilic
400 macrophages (MMMs), known to have immunological roles, may similarly exhibit a capacity for being
401 trained. This research can be further broadened to include other resident myeloid populations, to
402 explore how BCG can bestow localized protection independent of central HSC reprogramming.

403 When investigating the longevity of the trained transcriptional response within the spleen, we noted
404 that *Stat-1* and other interferon response genes remained upregulated even two months after
405 vaccination. We found one such gene SCA-1 (*Ly6A*), was continuously expressed in NCM due to training,
406 and was still identifiable after a BM transplant. Although SCA-1 is traditionally a marker for upstream
407 progenitors, recent studies link its expression to inflammation, with upregulation noted in B/T cells
408 during *Mycobacterium Tuberculosis* (Mtb) infection[49]. Further exploration is warranted to investigate the
409 mechanisms that enable such enduring expression, particularly in this cell type. Also, while *Ly6a* (SCA-1)
410 is unique to mice, a recent study identified a human equivalent termed *Ly6s*, primarily expressed in
411 splenic NCM and regulated by interferon signaling, that was linked to an inflammatory cell phenotype
412 with resistance to viral infections[50].

413 Prior publications have demonstrated the importance of BCG localization in generating local vs. systemic
414 changes[19,51], and that BCG's initial presence within the BM is associated with HSC reprogramming and
415 long-term TI. Despite this, while we were able to isolate BCG from splenic tissue, not BM, from all
416 sampled time points, we could still achieve training and protection, including LSK$^+$ subset expansion in
417 the BM. This leads us to hypothesize that the signaling initiated due to BCG can act in trans, affecting
418 system wide changes, and is not solely acquired due to local pathogen interactions in the BM.
419 Supporting this, recent findings suggest that training in alveolar macrophages can also occur through
420 subcutaneous BCG administration, potentially acting via the gut-lung axis[52].

421 Finally, given STAT1's ubiquity among all trained cells, we hypothesized that this transcription factor and
422 its upstream activation via interferon signaling were instrumental in driving BCG-induced trained

423 immunity. We observed that early transient inhibition, specifically targeting IFNγ-mediated STAT1
424 activation, effectively negated the hallmarks of trained immunity. These include myeloid recruitment,
425 disappearance of RPM, the expression of training markers, LSK^+ expansion, transcriptional alterations,
426 and, crucially, heterologous *S*. Tm protection. Furthermore, while it is generally known that BCG can
427 reside within the tissue for weeks after inoculation, our findings suggest that even brief STAT1 and IFNγ
428 inhibition is sufficient to disrupt the development of trained immunity, regardless of the pathogen's
429 presence. It is plausible that during the initial stages of BCG exposure and inflammation, IFNγ-secreting
430 cells such as T/NKTs initiate the immunological remodeling needed for training. Should these processes
431 be obstructed at this critical juncture, the opportunity for subsequent training is lost. While our inhibitor
432 protocol was applied for a period of five days, the minimal duration required for effective inhibition and
433 comparable outcomes may be even shorter.

434 In summary, our study emphasizes that examining the tissue, specifically the spleen, as a tissue for
435 probing TI offers valuable insights into the temporal dynamics and signaling cascades that instigate and
436 sustain TI locally, in parallel with established systemic effects. Central to these processes is the IFNγ-
437 STAT1 pathway, which we identified as a key driver in establishing TI, by replenishment of resident naïve
438 MPs with trained recruited and local immune populations. We further delineated that during
439 intraperitoneal vaccination the resultant immune interactions limit BCG dissemination, while still
440 effectively eliciting training. Our findings open new avenues to harness STAT1 pathway induction for
441 optimized training and heterologous protection.

442

443

444

445 # Methods

446 ## Experimental Methods

447 ### Mice and bacteria strains

448 C57BL/6J mice, 7-9 weeks old, were purchased from ENVIGO, housed at the Weizmann Institute
449 pathogen-free facility, and provided with standard food and water ad libitum. The Nr4a1 super-

450 enhancer sub-domain E2-KO ($E2^{-/-}$ or ^{C57BL}/6-*Rr39*^{em1Ched}/J) mice were purchased from The Jackson
451 Laboratory (#030204)[53]. The mice strains below were kindly provided by the following investigators:

452 - STAT1-KO mice by Prof. Dr. Mathias Müller[41].
453 - Ms4a3Cre^{TdTomato}-CX3CR1^{GFP} and CD45.1 mice by Prof. Steffen Jung.

454 All experiments were performed in accordance with the guidelines outlined by the Weizmann Institute
455 Committee on Animal Care.

456 For in-vivo training, BCG-Pasteur, generously donated by Dr. Daniel Barkan, was utilized. The *Salmonella*
457 *enterica* serovar Typhimurium strain SL1344 was used exclusively for all infection challenge experiments.

458 **Mice training and infection**

459 BCG were grown in Middlebrook 7H9 media (BD) supplemented with Middlebrook OADC (BD) at 37°C
460 for 1 week to stationary phase. Bacterial aliquots of 1mL were dispensed to 2mL cryotubes (Simport)
461 and frozen at -80C for long term storage. Prior to inoculation, tubes were thawed, centrifuged (10,000g,
462 2 min, RT), with pellet resuspended in 1 mL phosphate-buffered saline (PBS) (Sartorius). Bacterial
463 concentration was calculated based on optical density at 600nm (OD_{600}) assuming a concentration of
464 $5x10^8$ CFU/OD, with BCG diluted to $25x10^6$ CFU/mL in PBS. Mice were injected intraperitoneally (i.p)
465 with 200µl containing $5x10^6$ CFU or PBS (as controls). At given time points, mice were euthanized by CO_2,
466 spleens and/or BM from the femur were harvested, and CFU numbers were evaluated by plating serial
467 10-100-fold dilutions of homogenized spleens or BM suspension on selective 7H9-Middlebrook agar
468 plates.

469 For the initial challenge as observed in Fig.1A, cultures of S.*Tm* were grown in Luria-Bertani (LB) medium
470 (BD) at 37°C for 16 hours to stationary phase. For all subsequent experiments, S.*Tm* were grown at 37°C
471 for 16 hours to stationary phase in SPI-2 inducing media[54]: MgMES media (170 mM 2-(N-morpholino)
472 ethanesulfonic acid (MES) at pH 5.0, 5 mM KCl, 7.5 mM (NH4)2SO4, 0.5 mM K2SO4, 1 mM KH2PO4, 8
473 mM MgCl2, 38 mM glycerol, and 0.1% casamino acids. Cultures were centrifuged (10,000g, 2 min, RT),
474 with pellet resuspended in PBS. Bacteria were diluted 10-fold in PBS and concentration calculated based
475 on optical density at 600nm (OD_{600}). Assuming a concentration of $1x10^9$ CFU/OD, S.*Tm* was diluted to
476 $2.5x10^6$ CFU/mL in PBS. Mice were injected intraperitoneally (i.p) with 200 µl containing $1x10^5$ CFU of
477 bacteria or PBS (as controls). Injected bacterial load was verified by CFU. 24 hours post infection, mice

478 were euthanized by CO_2, spleens were harvested, and CFU numbers were evaluated by plating serial 10-
479 100-fold dilutions of homogenized spleens on streptomycin LB agar plates.

480 **BCG CFU**

481 Spleens or BM were homogenized and serially diluted in PBS + 0.1% Triton on 7H9 Middlebrook media +
482 OADC with Zeocin and Kanamycin. Plates were incubated for three weeks in a humidified 5% CO^2
483 incubator, with CFU determined using an automated colony counter.

484 **In-vivo interferon inhibition**

485 JAK-STAT inhibitors Fedratinib (cat #202893), and Deucravacitinib (cat #555349) (MedKoo Biosciences)
486 were resuspended in DMSO, aliquoted, and stored at -80C for later use. For injection, a mixture of PEG-
487 300 (Sigma):Tween-80 (Sigma) was prepared at a ratio of 18:1 and filtered using a 0.22 µm filter. For
488 each injection, 10µl of DMSO with or without the inhibitor was added to 105 µl of the PEG:Tween mix,
489 followed by 180µl of PBS for a total of 30µl and injected i.p. Inhibitor concentrations are 1mg and 0.5mg
490 per mouse for Fedratinib and Deucravacitinib respectively. Four hours post inhibitor, BCG or PBS-i.p was
491 injected for training. Daily repeat injections of the inhibitors were repeated for four additional days.

492 For the antibody inhibition experiment, 1mg of monoclonal αIFNγ antibody (clone: XMG1.2) or isotype
493 control (clone: Rat IgG1) was injected i.p. four hours pre BCG vaccination (day 0), then every other day
494 (day 2 and 4).

495 **Splenocytes and BM isolation and flow cytometry preparation**

496 Spleens and BM from femurs were extracted and stored in cooled FACS Buffer (PBS, 10 mM EDTA, 2%
497 FBS) until further extraction.

498 For BM extraction, femurs were cut at both ends and placed in 0.5mL microfuge tube with a small hole
499 in the bottom cut out using an 18G needle. This tube was then placed in a 1.5mL microfuge tube and
500 centrifuged (3 min, 500g, 4°C). The pellet was resuspended in red blood cell (RBC) lysis buffer for 4
501 minutes at room temperature, centrifuged (3 min, 500g, 4°C) and re-suspended with FACS buffer. For
502 CFU determination, suspension is used directly for serial dilution. For further flow cytometry processing,
503 FACS buffer containing CD16/CD32 blocking antibodies (BioLegend) is added for a 15-minute incubation
504 on ice. All subsequent processing is identical to splenocytes.

505 The spleens were dissected, mashed against a 70μm cell strainer (Falcon) and washed with 5mL of cold
506 FACS buffer. 1mL of splenocytes were aliquoted to microfuge tubes and centrifuged twice (3 min, 500g,
507 4C). Pellets were re-suspended with RBC lysis buffer (Sigma), incubated for 4 minutes at room
508 temperature, centrifuged (3 min, 500g, 4C) and re-suspended with FACS buffer containing CD16/CD32
509 blocking antibodies (BioLegend) for 15 minutes on ice. Cells were centrifuged once more, and pellets
510 were transferred to wells of a 96-well low attachment plate for multi-sample preparation. Subsequently,
511 fluorophore-conjugated antibodies cocktails (listed below) in Brilliant Stain Buffer (BD) were used to
512 resuspend pellets, followed by a 30-minute incubation on ice. Cells were washed, re-suspended with
513 500-1000μl FACS buffer and passed through a 35μm cell strainer (Falcon). For absolute quantification of
514 cell populations, 10-50μl of Precision Count beads (BioLegend) were added to the samples.

515

516

517

518

519

520 **Antibodies used in this study for splenocyte and BM staining**

Epitope	Conjugation	Clone	Company
CD16/CD32	NA	93	BioLegend
NK1.1	APC	PK136	BioLegend
CD19	APC	6D5	BioLegend
CD3	APC	17A2	BioLegend
Ly6G	APC	1A8	BioLegend
Ly6C	Alexa Fluor® 700™	HK1.4	BioLegend
Ly6C	Brilliant Violet 605™	HK1.4	BioLegend
CD11b	APC/Cy7	M1/70	BioLegend
CD11c	FITC	N418	BioLegend
CXCL9	PE	MIG-2F5.5	BioLegend

F4/80	PE	BM8	BioLegend
F4/80	Brilliant Violet 421™	BM8	BioLegend
I-A/I-E (MHC-II)	Brilliant Violet 605™	M5/114/15.2	BioLegend
Ly-6A/E (Sca-1)	PE/Cyanine7	E13-161.7	BioLegend
CD11c	PerCP/Cyanine5.5	N418	BioLegend
Ter-119	FITC	TER-119	BioLegend
CD4	FITC	GK1.5	BioLegend
CD8a	FITC	53-6.7	BioLegend
Gr-1	FITC	RB6-8C5	BioLegend
CD45R/B220	FITC	RA3-6B2	BioLegend
CD11b	FITC	M1/70	BioLegend
CD117/c-Kit	APC	2B8	BioLegend
Ly-6A/E (Sca-1)	PE-Vio 770™	REA422	Miltenyi

521

522

523

524 **Flow cytometry and sorting for RNA sequencing**

525 Flow cytometry and sorting was performed using the BD FACSAria III (BD). Single cells were sorted into
526 384-well plates (Eppendorf) containing 2µl of a solution containing barcoded poly-T primers for reverse
527 transcription (Sigma, Israel) according to the MARS-seq v2.0 protocol[55]. For bulk cell capture, 5-10x10^3
528 cells from each population were sorted into tubes containing 300µl RLT buffer (Qiagen) with β-
529 mercaptoethanol (BME). Immediately after sorting, plates or tubes were spun down, flash-frozen in a
530 mixture of dry ice and ethanol and stored in -80C until processing.

531 **Single-cell RNA-seq library preparation**

532 Single-cell libraries were prepared as described[55]. Briefly, mRNA from cells was converted to cDNA
533 alongside barcoding and UMI addition. The cDNA of each plate was pooled followed by second DNA
534 strand synthesis and T7 in vitro transcription. Amplified RNA was fragmented, followed by ligation of
535 partial P5 Illumina sequence, and converted to cDNA. Full sequence of barcoded P5 and P7 of P5 were

536 added by PCR for a sequence ready library. Final libraries were quantified for peak size and
537 concentration using the Agilent TapeStation and Qubit HS DNA Assay kit (Invitrogen), respectively.

538 **Bulk RNA-seq library preparation**

539 RNA was extracted and cleaned using the RNeasy mini kit (Qiagen) with DNaseI digestion. Libraries were
540 then prepared according to an in-house MARs-seq or CEL-seq protocol optimized for bulk RNA samples.
541 Final libraries were quantified for peak size and concentration using the TapeStation 4200 (Agilent) and
542 Qubit HS DNA Assay kit (Invitrogen), respectively.

543 **Library Sequencing**

544 Bulk and single cell libraries were diluted to a concentration of 1.8pM and run on the NextSeq platform
545 (Illumina) according to Illumina guidelines, with 75 reads for read1, and 15 reads for read2. A mean of
546 6M reads per library for the kinetics data; a mean of 12M reads per library for IFNγ inhibitor data; and a
547 mean of 3M reads per library for the MS4a3^{TdTm} bulk sorted population data.

548 **CD45.1/CD45.2 adoptive transfer**

549 C57BL/6J mice, expressing CD45.1 or CD45.2, were trained according to our standard protocol using BCG
550 or PBS, respectively. After two weeks, BM was isolated from the femur from both mice, resuspended in
551 PBS, and mixed in a 1:1 ratio. Recipient mice (WT C57/BL6J) were irradiated with a single dose of 950
552 cGy using an XRAD 320 machine (Precision X-Ray [PXI]) and reconstituted the next day via retro-orbital
553 injection of $5x10^6$ mixed donor BM cells/mouse in 200µl PBS. Mice were given 6 weeks to allow for
554 reconstitution and repopulation of the hematopoietic system.

555 **Flow cytometry, CFU, and spleen size analysis and quantification**

556 Flow cytometry data was analyzed using the FlowJo software.

557 For size quantification, spleens were imaged against a contrasting background, and two-dimensional
558 area was calculated using the ImageJ software.

559 All graphs quantifying the results from flow cytometry and CFU results were performed using R on
560 RStudio with the Tidyverse package[56].

561 **Bioinformatics Analysis**

562 **scRNA-seq data analysis**

563 **Data preprocessing**

564 MARS-seq pipeline[55] was used for demultiplexing, alignment to the genome (mm9), and gene counting
565 by unique molecular identifier (UMI). Overall, we sequenced 1536 cells (768 from control mouse and
566 768 from trained mouse), with 1474 median UMI count per cell and 668 median genes per cell.

567 **Data normalization and gene filtration**

568 Only genes with at least one UMI count detected in at least one cell were used. Data was normalized to
569 a library size factor. Factors were calculated by dividing total UMI counts in each cell to the median of
570 the total UMI counts across all cells. Data was transformed to log10 scale (log10(UMI count+1)). Cells
571 with less than 200 UMIs were excluded due to low coverage (24 cells, 9 from naïve mouse and 15 from
572 trained mouse). We filtered out cell cycle and ribosomal genes and selected the top 425 most variable
573 genes for further analysis. Variable genes were selected based on fitting of the data to a simple noise
574 model based on the genes mean expression and dispersion (coefficient of variance).

575 **Data clustering and annotations**

576 Principal component analysis (PCA) was performed on the variable genes, and the first 40 PCs were used
577 for downstream analysis for k-nearest neighbor (KNN)-graph, based on Euclidian distance in PC space.
578 Clustering was performed using Louvain community detection on the KNN-graph (k=20). Overall, we
579 obtained 7 clusters. Cluster identity was inferred using cluster-specific and manually selected genes
580 based on cell classification literature.

581 **Bulk RNA-seq data processing and normalization**

582 MARS-seq pipeline was used for samples demultiplexing, alignment to the genome (mm9), and gene
583 counting. Data was normalized to a library size factor. Factors were calculated by dividing the total
584 number of reads from each sample to the median total number of reads across all samples. These
585 procedures were done for each dataset alone.

586 **Kinetics data**

587 Data was transformed to log2 scale, and minimal expression threshold was set to 3. Replicate samples of
588 each condition were averaged, except for 1 sample that was excluded due to low coverage (<100k
589 reads; BCG 30d replicate 3). Preceding PCA analysis genes were centered and normalized to a mean of 0
590 and a standard deviation of 1. To identify genes that were up-regulated due to training we calculated

591 the differences between the integrals of each gene in BCG relative to PBS along time. The differences
592 across all genes were approximately normally distributed, with a mean of 0.2 and a standard deviation
593 of 10.11. Genes with more than 3 standard deviations above the mean were defined as up-regulated
594 due to training.

595 **Bulk inhibitor data**

596 Data was transformed to log2 scale, and minimal expression threshold was set to 3. Two Fedratinib
597 samples were excluded from analysis due to technical issues during injection that resulted in a lack of
598 inhibition. Heatmap was generated using DEGs calculated by ANOVA (5% FDR and a minimal 2-fold; 167
599 genes).

600 **Fedratinib inhibitor data**

601 Data was transformed to log2 scale, and minimal expression threshold was set to 4. One sample was
602 excluded due to low coverage (<100k reads; PBS +S.*Tm* + Fedratinib replicate 3). Preceding PCA analysis
603 genes were centered and normalized to a mean of 0 and a standard deviation of 1. PCA analysis was
604 performed on DEGs calculated using two-sided t-tests between all relevant conditions: control vs.
605 trained samples, trained with or without inhibitor, control with or without inhibitor, uninfected vs.
606 infected, infected with or without training, infected vs. infected with training with inhibitor, and infected
607 with training vs. infected with training with inhibitor (5% FDR; 453 genes). Heatmap was generated using
608 two-sample t-test between control and BCG-trained samples (1% FDR).

609 **αIFNγ inhibitor data**

610 Data was transformed to log2 scale, and minimal expression threshold was set to 3. Two sample was
611 excluded due to low coverage (<250k reads CM BCG + Isotype replicate 1 and RPM BCG + Isotype
612 replicate 4). Heatmap genes were selected from cluster I and II from the lineage tracing experiment
613 representing shared interferon/STAT-1 upregulated genes.

614 **MS4A3^{Tdtm} bulk population data**

615 Data was transformed to log2 scale, and minimal expression threshold was set to 3. One sample was
616 excluded due to low coverage (<150k reads; control NCM-Tdtm^{+} replicate 4). Preceding PCA analysis
617 genes were centered and normalized to a mean of 0 and a standard deviation of 1. DEGs between

618 control and trained mice were calculated using two-sided t-test between all control samples versus all
619 trained samples (from all sorted populations together; 10% FDR, 382 genes).

620

621 Acknowledgments

622 This research was supported by the Israel Science Foundation (ISF grant No. 1289/22), the Minerva
623 Foundation with funding from the Federal Ministry for Education and Research, the Dr. Barry Sherman
624 Institute for Medicinal Chemistry, and the Shimon and Golde Picker Weizmann Annual Grant.

625

626 ## References

627

628 1. Arts, R. J. W. *et al.* Long-term in vitro and in vivo effects of γ-irradiated BCG on innate and adaptive
629 immunity. *Journal of Leukocyte Biology* **98**, 995–1001 (2015).
630 2. Saeed, S. *et al.* Epigenetic programming of monocyte-to-macrophage differentiation and trained
631 innate immunity. *Science* **345**, 1251086 (2014).
632 3. Darrah, P. A. *et al.* Prevention of tuberculosis in macaques after intravenous BCG immunization.
633 *Nature* **577**, 95–102 (2020).
634 4. Moorlag, S. J. C. F. M., Arts, R. J. W., van Crevel, R. & Netea, M. G. Non-specific effects of BCG
635 vaccine on viral infections. *Clinical Microbiology and Infection* **25**, 1473–1478 (2019).
636 5. Kurotaki, D., Uede, T. & Tamura, T. Functions and development of red pulp macrophages.
637 *Microbiology and Immunology* **59**, 55–62 (2015).
638 6. Hoeffel, G. *et al.* C-Myb(+) erythro-myeloid progenitor-derived fetal monocytes give rise to adult
639 tissue-resident macrophages. *Immunity* **42**, 665–678 (2015).
640 7. Lai, S. M. *et al.* Organ-Specific Fate, Recruitment, and Refilling Dynamics of Tissue-Resident
641 Macrophages during Blood-Stage Malaria. *Cell Reports* **25**, 3099-3109.e3 (2018).
642 8. Zhang, L. *et al.* Variable Virulence and Efficacy of BCG Vaccine Strains in Mice and Correlation With
643 Genome Polymorphisms. *Molecular Therapy* **24**, 398–405 (2016).
644 9. Review of the macrophage disappearance reaction - Barth - 1995 - Journal of Leukocyte Biology -
645 Wiley Online Library. https://jlb.onlinelibrary.wiley.com/doi/abs/10.1002/jlb.57.3.361.
646 10. Keren-Shaul, H. *et al.* MARS-seq2.0: an experimental and analytical pipeline for indexed sorting
647 combined with single-cell RNA sequencing. *Nat Protoc* **14**, 1841–1862 (2019).
648 11. Hu, X. & Ivashkiv, L. B. Cross-regulation of Signaling and Immune Responses by IFN-γ and STAT1.
649 *Immunity* **31**, 539–550 (2009).

650 12. Li, X. *et al.* GBP2 promotes M1 macrophage polarization by activating the notch1 signaling pathway
651 in diabetic nephropathy. *Front. Immunol.* **14**, (2023).
652 13. Meunier, E. *et al.* Caspase-11 activation requires lysis of pathogen-containing vacuoles by IFN-
653 induced GTPases. *Nature* **509**, 366–370 (2014).
654 14. Groom, J. R. & Luster, A. D. CXCR3 ligands: redundant, collaborative and antagonistic functions.
655 *Immunol Cell Biol* **89**, 207–215 (2011).
656 15. Joosten, S. A. *et al.* Mycobacterial growth inhibition is associated with trained innate immunity. *The*
657 *Journal of Clinical Investigation* **128**, 1837 (2018).
658 16. Michelucci, A. *et al.* Immune-responsive gene 1 protein links metabolism to immunity by catalyzing
659 itaconic acid production. *Proc Natl Acad Sci U S A* **110**, 7820–7825 (2013).
660 17. Lampropoulou, V. *et al.* Itaconate Links Inhibition of Succinate Dehydrogenase with Macrophage
661 Metabolic Remodeling and Regulation of Inflammation. *Cell Metab* **24**, 158–166 (2016).
662 18. Domínguez-Andrés, J. *et al.* The Itaconate Pathway Is a Central Regulatory Node Linking Innate
663 Immune Tolerance and Trained Immunity. *Cell Metabolism* **29**, 211-220.e5 (2019).
664 19. Kaufmann, E. *et al.* BCG Educates Hematopoietic Stem Cells to Generate Protective Innate Immunity
665 against Tuberculosis. *Cell* **172**, 176-190.e19 (2018).
666 20. Yang, S.-H. *et al.* IFN-γ–STAT1–iNOS Induces Myeloid Progenitors to Acquire Immunosuppressive
667 Activity. *Frontiers in Immunology* **8**, (2017).
668 21. Biram, A. *et al.* Bacterial infection disrupts established germinal center reactions through monocyte
669 recruitment and impaired metabolic adaptation. *Immunity* **55**, 442-458.e8 (2022).
670 22. Penton-Rol, G. *et al.* Selective Inhibition of Expression of the Chemokine Receptor CCR2 in Human
671 Monocytes by IFN-γ1. *The Journal of Immunology* **160**, 3869–3873 (1998).

672 23. Wang, Y. *et al.* Bacillus Calmette–Guérin–induced interleukin-10 inhibits S100A8/A9 production and
673 hinders development of T helper type 1 memory in mice. *European Journal of Immunology* **53**,
674 2250204 (2023).
675 24. Liu, K. *et al.* Neutrophilic granule protein (NGP) attenuates lipopolysaccharide-induced
676 inflammatory responses and enhances phagocytosis of bacteria by macrophages. *Cytokine* **128**,
677 155001 (2020).
678 25. Khan, N. *et al.* M. tuberculosis Reprograms Hematopoietic Stem Cells to Limit Myelopoiesis and
679 Impair Trained Immunity. *Cell* **183**, 752-770.e22 (2020).
680 26. Hoffman, D. *et al.* A non-classical monocyte-derived macrophage subset provides a splenic
681 replication niche for intracellular Salmonella. *Immunity* **54**, 2712-2723.e6 (2021).
682 27. Yona, S. *et al.* Fate mapping reveals origins and dynamics of monocytes and tissue macrophages
683 under homeostasis. *Immunity* **38**, 79–91 (2013).
684 28. Bomfim, C. C. B. *et al.* Mycobacterium tuberculosis Induces Irg1 in Murine Macrophages by a
685 Pathway Involving Both TLR-2 and STING/IFNAR Signaling and Requiring Bacterial Phagocytosis.
686 *Front Cell Infect Microbiol* **12**, 862582 (2022).
687 29. Tretina, K., Park, E.-S., Maminska, A. & MacMicking, J. D. Interferon-induced guanylate-binding
688 proteins: Guardians of host defense in health and disease. *J Exp Med* **216**, 482–500 (2019).
689 30. Clement, M. *et al.* IFITM3 restricts virus-induced inflammatory cytokine production by limiting
690 Nogo-B mediated TLR responses. *Nat Commun* **13**, 5294 (2022).
691 31. Carow, B. *et al.* Critical and independent role for SOCS3 in either myeloid or T cells in resistance to
692 Mycobacterium tuberculosis. *PLoS Pathog* **9**, e1003442 (2013).
693 32. Vogt, A.-C. S. *et al.* On Iron Metabolism and Its Regulation. *International Journal of Molecular*
694 *Sciences* **22**, 4591 (2021).

695 33. Liu, Z. *et al.* Fate Mapping via Ms4a3-Expression History Traces Monocyte-Derived Cells. *Cell* **178**,
696 1509-1525.e19 (2019).
697 34. Yáñez, A. *et al.* Granulocyte-Monocyte Progenitors and Monocyte-Dendritic Cell Progenitors
698 Independently Produce Functionally Distinct Monocytes. *Immunity* **47**, 890-902.e4 (2017).
699 35. De Leon-Oliva, D. *et al.* AIF1: Function and Connection with Inflammatory Diseases. *Biology (Basel)*
700 **12**, 694 (2023).
701 36. Prevete, N., Liotti, F., Marone, G., Melillo, R. M. & de Paulis, A. Formyl peptide receptors at the
702 interface of inflammation, angiogenesis and tumor growth. *Pharmacol Res* **102**, 184–191 (2015).
703 37. Gibbings, D. J., Marcet-Palacios, M., Sekar, Y., Ng, M. C. Y. & Befus, A. D. CD8 alpha is expressed by
704 human monocytes and enhances Fc gamma R-dependent responses. *BMC Immunol* **8**, 12 (2007).
705 38. Sugimoto, M. A., Vago, J. P., Teixeira, M. M. & Sousa, L. P. Annexin A1 and the Resolution of
706 Inflammation: Modulation of Neutrophil Recruitment, Apoptosis, and Clearance. *J Immunol Res*
707 **2016**, 8239258 (2016).
708 39. Håversen, L. *et al.* Vimentin deficiency in macrophages induces increased oxidative stress and
709 vascular inflammation but attenuates atherosclerosis in mice. *Sci Rep* **8**, 16973 (2018).
710 40. Karlstetter, M. *et al.* The Novel Activated Microglia/Macrophage WAP Domain Protein, AMWAP,
711 Acts as a Counter-Regulator of Proinflammatory Response. *The Journal of Immunology* **185**, 3379–
712 3390 (2010).
713 41. Kernbauer, E. *et al.* Conditional Stat1 Ablation Reveals the Importance of Interferon Signaling for
714 Immunity to Listeria monocytogenes Infection. *PLoS Pathog* **8**, e1002763 (2012).
715 42. Lé, A. M., Puig, L. & Torres, T. Deucravacitinib for the Treatment of Psoriatic Disease. *Am J Clin*
716 *Dermatol* **23**, 813–822 (2022).
717 43. Kalafati, L. *et al.* Innate Immune Training of Granulopoiesis Promotes Anti-tumor Activity. *Cell* **183**,
718 771-785.e12 (2020).

719 44. Huijser, E. *et al.* Trained Immunity in Primary Sjögren's Syndrome: Linking Type I Interferons to a
720 Pro-Atherogenic Phenotype. *Frontiers in Immunology* **13**, (2022).
721 45. Zahalka, S. *et al.* Trained immunity of alveolar macrophages requires metabolic rewiring and type 1
722 interferon signaling. *Mucosal Immunol* **15**, 896–907 (2022).
723 46. Moorlag, S. J. C. F. M. *et al.* β-Glucan Induces Protective Trained Immunity against Mycobacterium
724 tuberculosis Infection: A Key Role for IL-1. *Cell Reports* **31**, 107634 (2020).
725 47. Liao, C., Prabhu, K. S. & Paulson, R. F. Monocyte-derived macrophages expand the murine stress
726 erythropoietic niche during the recovery from anemia. *Blood* **132**, 2580–2593 (2018).
727 48. Haldar, M. *et al.* Heme-mediated SPI-C induction promotes monocyte differentiation into iron-
728 recycling macrophages. *Cell* **156**, 1223–1234 (2014).
729 49. Akter, S. *et al.* Mycobacterium tuberculosis infection drives a type I IFN signature in lung
730 lymphocytes. *Cell Reports* **39**, 110983 (2022).
731 50. Shmerling, M. *et al.* LY6S, a New IFN-Inducible Human Member of the Ly6a Subfamily Expressed by
732 Spleen Cells and Associated with Inflammation and Viral Resistance. *ImmunoHorizons* **6**, 253–272
733 (2022).
734 51. Vierboom, M. P. M. *et al.* Stronger induction of trained immunity by mucosal BCG or MTBVAC
735 vaccination compared to standard intradermal vaccination. *Cell Rep Med* **2**, 100185 (2021).
736 52. Jeyanathan, M. *et al.* Parenteral BCG vaccine induces lung-resident memory macrophages and
737 trained immunity via the gut–lung axis. *Nat Immunol* **23**, 1687–1702 (2022).
738 53. Thomas, G. D. *et al.* Deleting an Nr4a1 Super-Enhancer Subdomain Ablates Ly6Clow Monocytes
739 while Preserving Macrophage Gene Function. *Immunity* **45**, 975–987 (2016).
740 54. Stapels, D. A. C. *et al.* Salmonella persisters undermine host immune defenses during antibiotic
741 treatment. *Science* **362**, 1156–1160 (2018).

742 55. MARS-seq2.0: an experimental and analytical pipeline for indexed sorting combined with single-cell
743 RNA sequencing | Nature Protocols. https://www.nature.com/articles/s41596-019-0164-4.
744 56. Wickham, H. *et al.* Welcome to the Tidyverse. *Journal of Open Source Software* **4**, 1686 (2019).
745
746

747 # Figures and legends

Figure 1

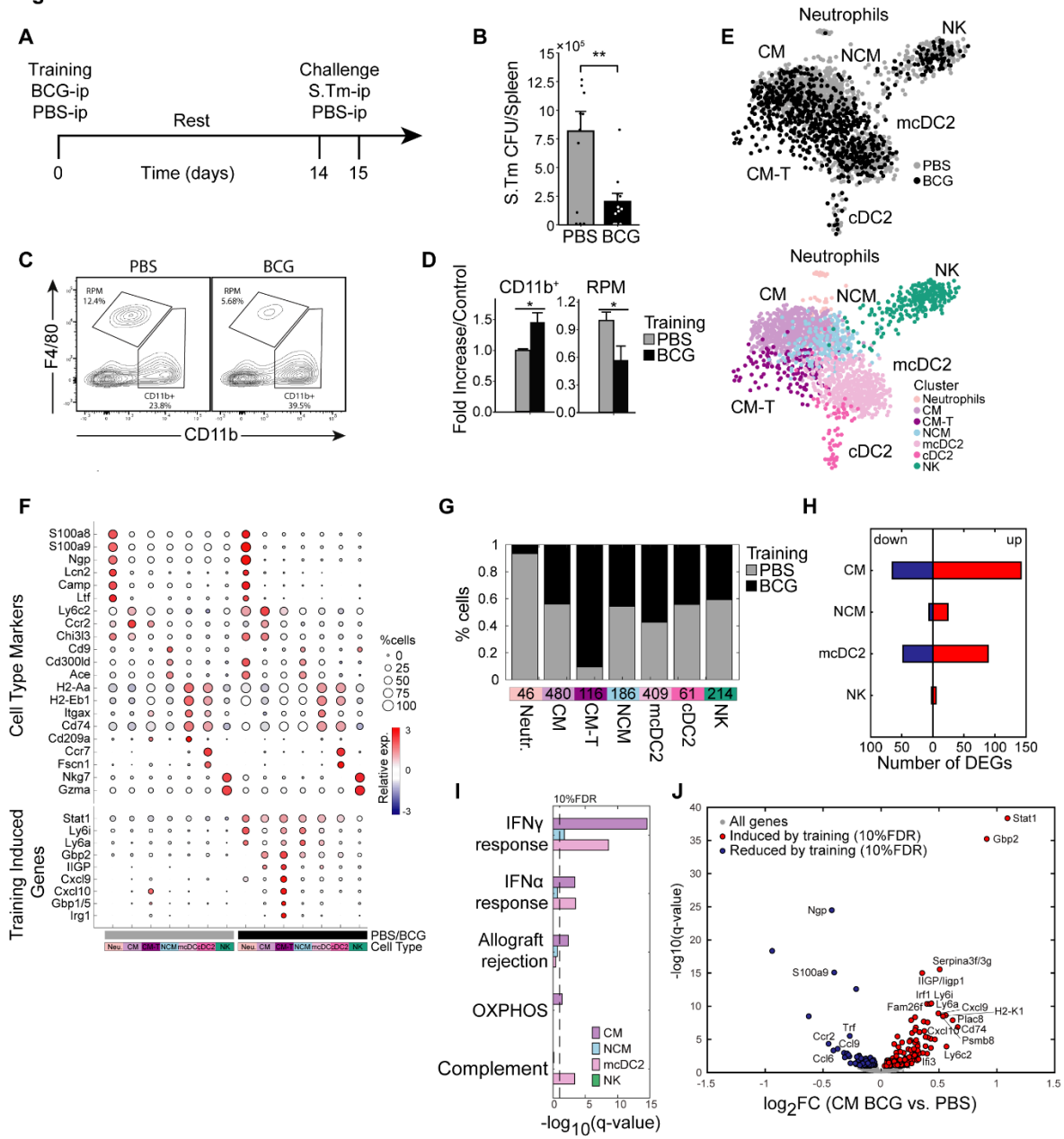

748

749 **Figure 1. Intraperitoneal BCG results in heterologous *S*.Tm protection and a distinct myeloid subsets**
750 **with signatures driven by STAT1.** (**A**) Experimental schema of in-vivo training. (**B**) Splenic S.*Tm* CFU 24
751 hours post infection between control (n=11) and trained mice (n=11). (**C-D**) Flow cytometry plots of
752 myeloid populations (C) and mean percentage fold change of BCG over control for each given gated
753 population percent from the Lin$^-$ population (D). (**E**) K-nearest neighbors (KNN) plot for total CD11b$^+$
754 single cells sorted from control and BCG mice. Color is based on conditions, or cluster identity. (**F**) Cell
755 markers and training induced genes for each subset. Size and color intensity indicates percentage of
756 cells within a given cluster expressing the gene and average expression. (**G**) Proportions of monocyte
757 subsets based on classifications in E. (**H-I**) Number of DEGs in each cell subset (H), and their

758 corresponding gene set enrichment analysis (I). (**J**) Volcano plot of DEGs in CM-T subset. Data in bar
759 graphs are presented as mean±SEM, with each individual point in **B** a biological repeat. Two-tailed *t*-test
760 used for data in **B** and **D** (**P*<0.05, ***P*<0.01).

761

762

Figure 2

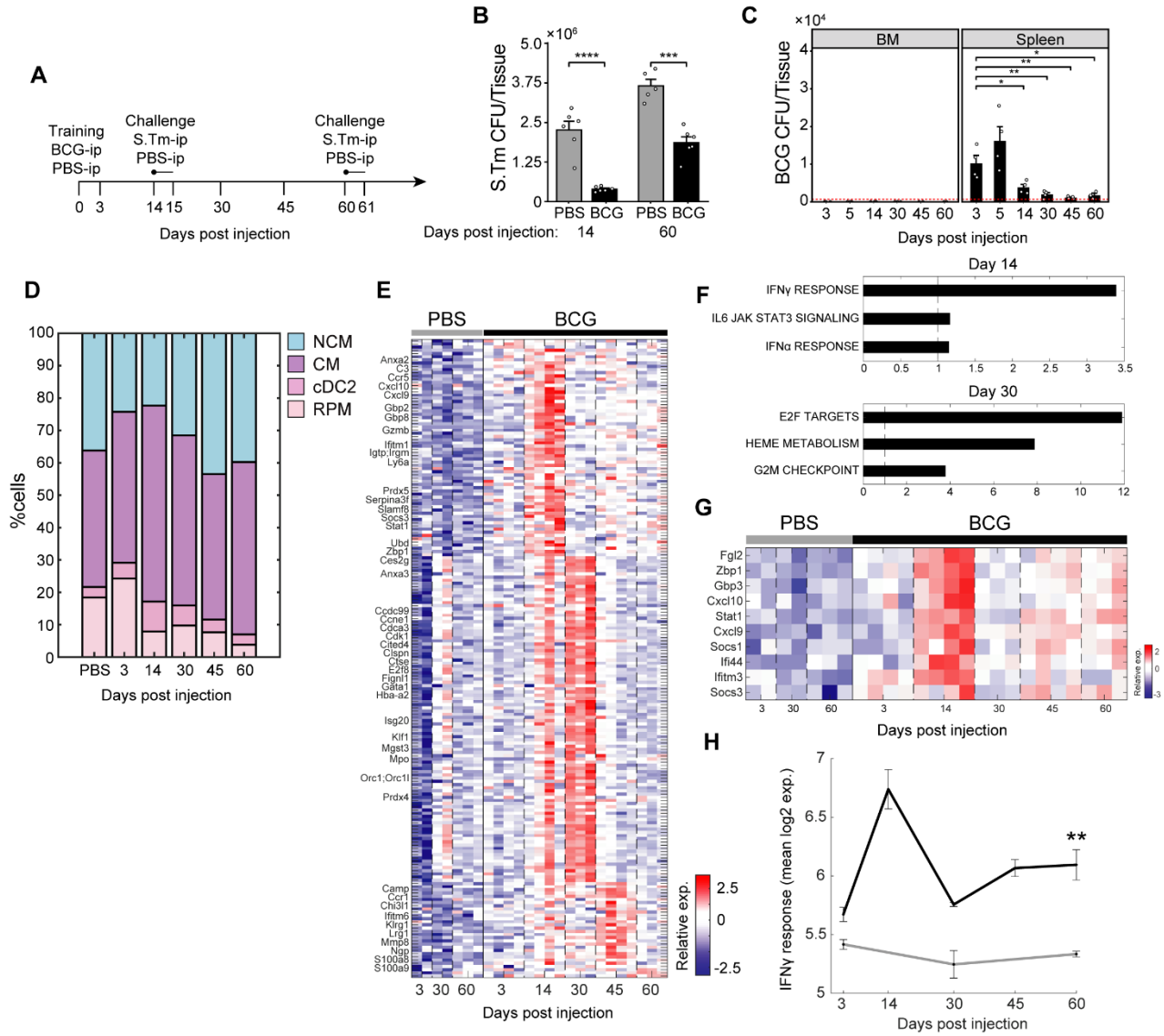

763

764 **Figure 2. Dynamics of TI-associated subsets and signatures indicates early and delayed kinetics.** (**A**)
765 Experimental schema tracking TI kinetics over a two-month interval. (**B**) Splenic *S.Tm* CFU at 24 hours
766 post infection for control and BCG mice at 14- and 60- days after inoculation (n=5-6). (**C**) BCG CFU from
767 spleen and BM of BCG inoculated mice (n=4) across time points. Red-dotted line indicates limit of
768 detection. (**D**) MP populations from control (PBS) and BCG mice (days post injection). Percentage of CM,
769 NCM, and dendritic cells calculated from flow cytometry analysis of $CD11b^+$ population. Percentage of
770 RPM calculated from Lin^- population (control: n=3, BCG: n=4 in each time point). PBS values are the
771 mean of all time points. (**E**) Heatmap of upregulated genes due to training and relative gene expression
772 ordered according to peak expression time. (**F**) Gene set enrichment analysis of DEGs in days 14 and 30.
773 (**G-H**) Heatmap of IFNγ response genes (G) and their average expression dynamics (H). Data in bar and
774 line graphs are presented as mean±SEM. For bar graph **B** and **C**, each individual point is a biological

775 repeat. For line graph **H**, significance represents comparison between day 60 control and BCG. Heatmap
776 rows in **E** and **G** indicate biological replicates. Two-tailed *t*-test used for data in **B**, **C**, and **H (***$P<0.05$,
777 ****$P<0.01$, *****$P<0.005$, ******$P<0.001$**)**.

778

Figure 3

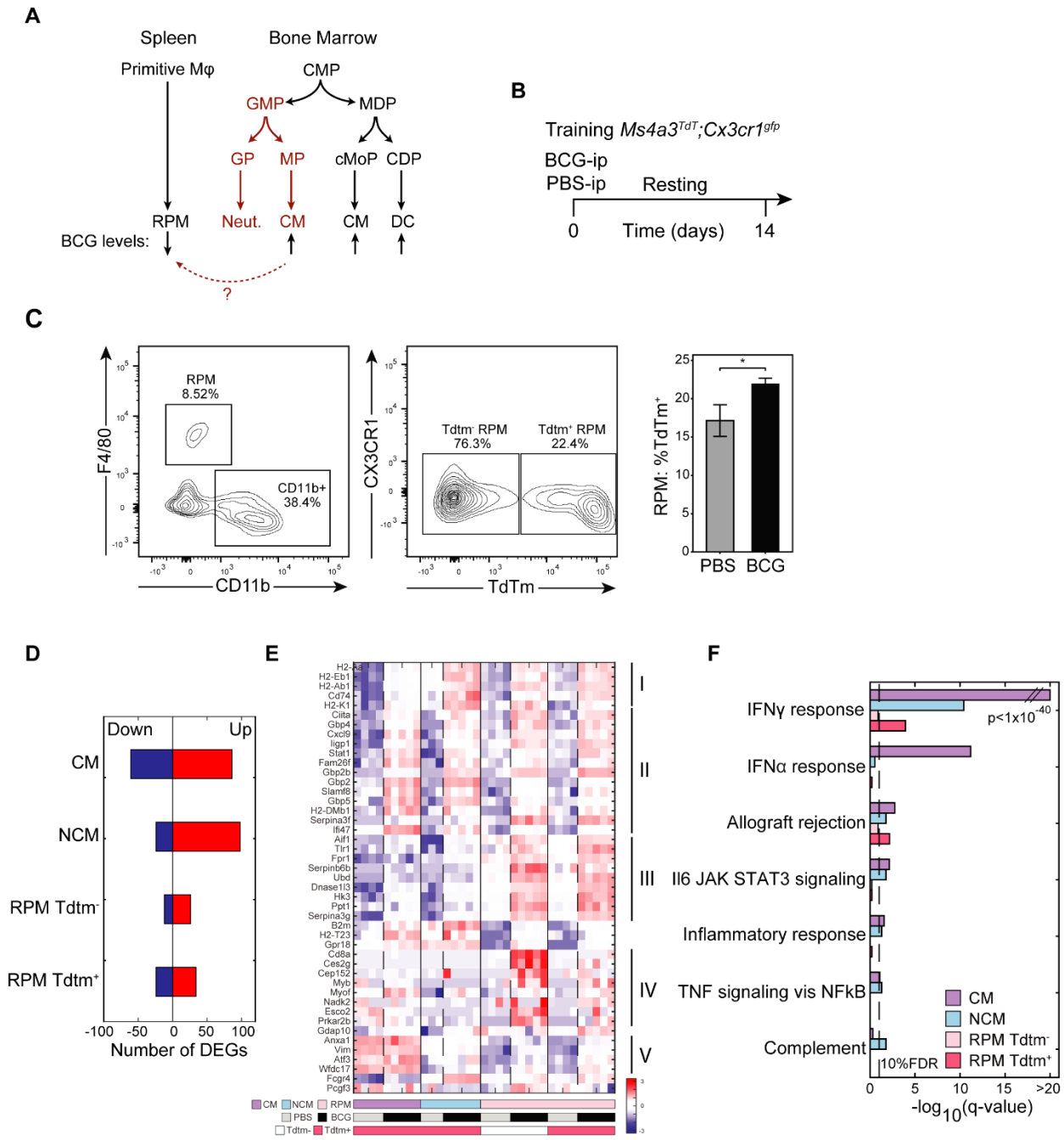

Figure 3. RPM niche is replenished by recruited trained monocytes and by local training of tissue-resident populations. (**A**) Scheme representing known myeloid differentiation pathways and potential trans-differentiation of trained CM to RPM. (**B**) Experimental schema for lineage tracing of TI-associated MP populations. (**C-D**) Flow cytometry analysis of TdTm$^+$ or Tdtm$^-$ Ly6C$^+$ MPs and RPM and quantification of RPM TdTm$^+$ subset (n=3). (**D-F**) Number of DEGs of each sorted population (D),

786 heatmap of normalized log2 expression from TI-associated DEGs specific to trained RPM populations
787 and gene set enrichment analysis of DEGs in each sorted population (F). Data in bar graphs are
788 presented as mean±SEM. Heatmap rows in **E** indicate biological replicates. Two-tailed *t*-test used for
789 data in **C** (*P<0.05).

790

Figure 4

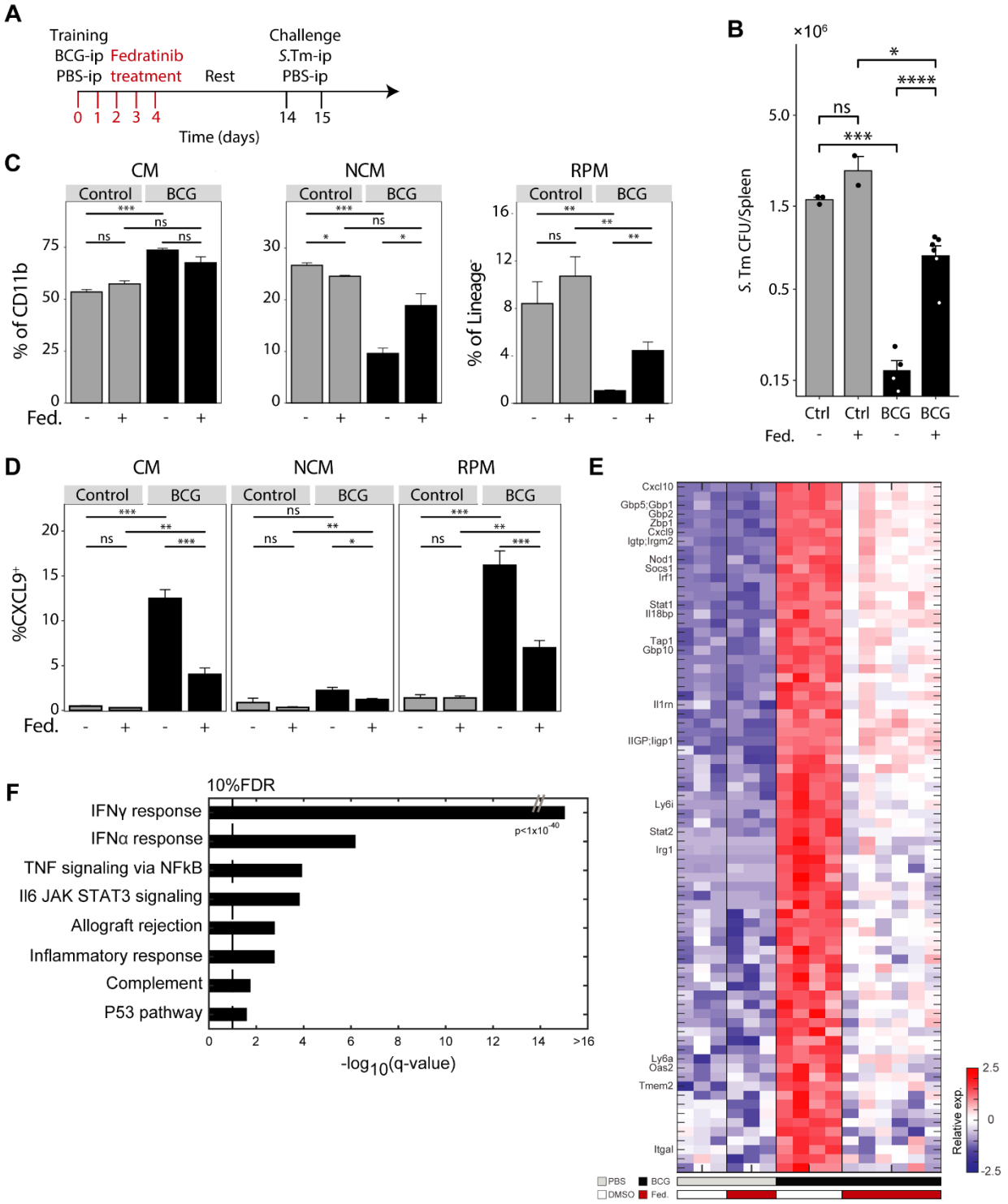

Figure 4. Transient IFNγ-STAT1 inhibition prevents TI signatures and splenic infection resistance. (**A**) Experimental schema of training with early treatment of Fedratinib inhibitor. (**B**) Splenic S.*Tm* CFU for

795 control and BCG mice, with and without Fedratinib inhibitor, 24h post infection (n=2-6).(**C**) MP
796 populations from control (gray) and BCG (black) mice, with or without Fedratinib inhibition. Percentage
797 of CM and NCM cells calculated from $CD11b^+$ population. Percentage of RPM calculated from Lin^-
798 population. (**D**) Percentage of CM, NCM, and RPM populations expressing CXCL9 from control (gray) and
799 BCG (black) mice, with or without Fedratinib inhibition (control: n=3, BCG: n=4, control+Fedratinib: n=3,
800 BCG+Fedratinib: n=6). (**E**) Heatmap of normalized log2 expression of DEGs across naïve and training
801 conditions. (**F**) Gene set enrichment analysis of DEGs from E. Data in bar graphs are presented as
802 mean±SEM. For bar graph **B** each individual point is a biological repeat. Heatmap rows in E indicate
803 biological replicates. Two-tailed *t*-test used for data in **B**, **C**, and **D** (*P<0.05, **P<0.01, ***P<0.005,
804 ****P<0.001**)**.

805